Available online at www.sciencedirect.com
SCIENCE DIRECT®
Journal of Chromatography A, 1023 (2004) 143–150
JOURNAL OF CHROMATOGRAPHY A
www.elsevier.com/locate/chroma

In-channel dual-electrode amperometric detection in electrophoretic chips with a palladium film decoupler

Chi-Chung Joseph Lai [a,1], Chun-hsien Chen [a,*], Fu-Hsiang Ko [b,*,2]

[a] *Department of Chemistry, National Tsing Hua University, Hsinchu, Taiwan 30013, ROC*
[b] *National Nano Device Laboratories, 1001-1 Ta-Hsueh Road, Hsinchu, Taiwan 30050, ROC*

Received 6 August 2003; received in revised form 8 September 2003; accepted 23 September 2003

Abstract

An electrophoretic microchip integrated with a Pd-film decoupler and a series-dual electrode was proven practical (200–800 V/cm) for routine amperometric detection. In fluidic systems, amperometric enhancement of parallel-opposed dual-electrode detection is due to redox cycling of analytes between the electrodes. We, however, found that the oxidation current of catecholamines was enhanced significantly (1.9–3.8 folds) by switching from the single electrode mode to dual-series mode. This novel finding was unexpected because the unidirectional flow characteristic of the microfluidic system should eliminate the possibility for analytes physically migrating back and forth between the upstream and downstream electrodes. We attribute the enhancement to turbulence generated by impinging of the flow onto the edge of the downstream electrode. The linear range, sensitivity, limit of detection (S/N = 3) and number of theoretical plates for DA and CA are, respectively, 0.5–50 μM, 47 pA/μM, 0.25 μM, 7000 m^{-1}, and 1.0–100 μM, 28 pA/μM, 0.49 μM, 15 000 m^{-1}.

Keywords: Palladium film decoupler; Dual-electrode detection; Chip technology; Amperometric detection

1. Introduction

For separation techniques such as liquid chromatography [1–3] and electrophoresis [3–17], it has been acknowledged that electrochemical (EC) detection with two working electrodes is superior to single-electrode mode in terms of selectivity and sensitivity. With respect to the flow pathway, the two electrodes have been configured in series, in parallel, and with the electrodes parallel-opposed [1–3]. Among these configurations, the most common one is the series mode in which analytes pass across one electrode and then the other. The upstream electrode can generate electroactive species or screen out the EC irreversible interferants for the downstream electrode. The upstream and downstream electrodes are usually termed generator and collector, respectively, because the reaction product of an EC reversible species is generated at the upstream electrode and the corresponding amperometric signal of that product is collected at the downstream electrode.

Research on fabrication and applications of microfluidic chip has been flourishing since the pioneering work by Harrison et al. [18,19]. The miniaturized devices have the capacity of incorporating sample preparation, injection, separation, derivatization, and detection into one small chip. Over the past decade, numerous materials have been discovered suitable for the microfabrication processes [20]. The microchip devices are thus not restrictedly limited to laboratories with standard lithographic facilities and have generated a great deal of interest. The dimension of microfluidic chips is particularly suitable to capillary electrophoresis which requires exceptionally small sample volumes, consumes minimal solvent, and exhibit excellent separation efficiency. EC detection has several advantages for operation with microchip electrophoresis systems, for example, ease of miniaturization, high sensitivity, and selectivity. Therefore, electrophoretic applications of microfluidic chips integrated with EC detection has gained wide acceptance [21–40].

We recently reported a design of amperometric detection for electrophoretic chips in which the working electrodes were placed within the separation channel [40]. A palladium metallic film was employed as the ground electrode for

* Corresponding authors. Tel.: +886-3-573-7009; fax: +886-3-571-1082.
E-mail addresses: chhchen@mx.nthu.edu.tw (C.-h. Chen), fhko@ndl.gov.tw (F.-H. Ko).
[1] Tel.: +886-3-573-7009; fax: +886-3-571-1082.
[2] Tel.: +886-3-572-6100x7618; fax: +886-3-572-2715.

0021-9673/$ – see front matter © 2003 Elsevier B.V. All rights reserved.
doi:10.1016/j.chroma.2003.09.053

electrophoresis and utilized to decouple the electric circuitry of the electrophoretic separation from that of the electrochemical detection. A few research groups have demonstrated the effectiveness of Pd as a decoupler [4,40–42] and the rationale has been elucidated by Kok and Sahin [41], and Huang and Kok [42]. In brief, Pd is permeable to hydrogen whose diffusion coefficient in bulk Pd is approximately 2×10^{-7} to 3×10^{-7} cm^2 s^{-1} at room temperature [43–45]. Under the high electric field of electrophoresis, hydrolysis of water results in production of hydrogen which adsorbs onto the Pd surface and then diffuses into bulk phase. For a tubular decoupler with length, inner and outer radii of 1.0, 0.1 and 1.5 mm, respectively, Kok and Sahin estimated that the amount of hydrogen dissipation via the Pd decoupler corresponds to 500 μA, two orders of magnitude higher than typical electrophoretic current (10–100 μA) [41]. The high diffusion coefficient warrants elimination of bubbles resulting from hydrogen evolution at the ground electrode within the separation channel, which would otherwise become a detrimental problem for capillary electrophoresis. Recently, the concept of utilizing a metallic film decoupler in CE–EC is further demonstrated by Chang and co-workers [38]. In their study a platinized film is employed as the decoupler and a three-electrode EC detection system was located within the separation channel.

In our previous work on the Pd-film decoupler, the channels of the electrophoretic chip were generated by thermal imprinting of tungsten wires on a piece of Plexiglas [40,46–48]. The shape and dimensions of the channels were ill-defined and thus we were not able to provide detail information regarding hydrogen dissipation under regular CE conditions. In the work presented here, the channels were better defined because the microfluidic chips were prepared by casting an elastomeric material, poly[dimethylsiloxane] (PDMS), against a cross-shaped positive relief manufactured by the standard photolithographic method [49]. The slab of PDMS, consisting of microfluidic channels, was then activated by oxygen plasma treatment and bonded with a piece of glass slide pre-patterned metallic film electrodes for electrophoresis and EC detection. In the following, we first describe the performance of the Pd decoupler under a range of ordinary CE electric fields and common electrolytes. We then extend the application of our previous study to dual-electrode amperometric detection. Surprisingly, the signal at the upstream electrode is affected by the potential setting at the downstream electrode. The collection efficiency (defined as the faradaic current at the downstream electrode divided by the current at the upstream electrode) is as high as 60%.

2. Experimental

2.1. Preparation of microfluidic chips

The preparation procedures were based on the method developed by Whitesides and co-workers [49]. Described in the following are the preparation of the positive relief, PDMS replica, substrates of glass slides with metallic films for electrophoresis and electrochemistry, and bonding procedures for the microfluidic chips.

2.1.1. Preparation of positive relief (masters for PDMS)

The imprinting mold was fabricated with a series of processes. The square glass (Hoya-5009, 127 mm × 127 mm) coated with chromium layer and chromium oxide layer was purchased from Hoya Company (Tokyo, Japan). The Shipley negative resist (SAL-601, Tokyo, Japan) was dispensed onto the glass and spun (Convac-801 spin coater, Illingen, Germany) at the rate of 50 rps for 1 min, followed by soft baking on a 105 °C Convac hot-plate for 10 min. The resist film thickness was 830 nm. The resist composition provided from the vendor was 79–81% 1-methoxy-2-propyl acetate, 19–21% melamine and novolak resin, and <1% acid generator. The characteristic reaction of the negative resist was cross-linkage after suitable electron beam exposure, which was carried out on Jeol JBX-5DII electron beam lithography system (Tokyo, Japan) at the dose of 2.4 μC/cm^2 and followed by post exposure baking on a 105 °C Convac hot-plate for 10 min. The electron beam energy was 25 keV with beam size of 500 nm and beam current of 1 nA. The unexposed resist on the glass was then dissolved with developer (MF-312, Shipley Company) for 1 min, followed by water cleaning. The developer was an aqueous solution containing 4.5% tetramethylammonium hydroxide. The development process was repeated twice by Convec CPP-70 machine, followed by hard baking on a 105 °C Convac hot-plate for 10 min. After resist pattern revealing, the chromium and chromium oxide layers on the glass were etched with wet chemical (CR-7T, Cyantek Corporation, CA, USA) by Convec CPP-70 machine. The etching chemical was an aqueous solution containing 9% $Ce(NH_4)_2(NO_3)_6$ and 6% $HClO_4$. Finally, the residual resist was removed by the 3:1 mixture of H_2SO_4 and H_2O_2 at 105 °C for 10 min.

The photoresist-patterned glass was immersed in a 600 ml diluted HF solution (1:1 ratio of water to 50% HF). The positive relief was created because the patterned area was protected by the chrome adlayer while the surrounding bare glass was etched away. The etching rate was found 17 μm/min and was used to control the height of the pattern. Note that the rate decreased associated with the freshness of the HF solution. The height of the positively raised structure, equivalent to the depth of the channels in the PDMS, was examined with an α-step profilometer (for example, Fig. 1D and E) (Dektak 3030, Sloan Technology Corp, Santa Barbara, CA, USA).

2.1.2. Preparation of PDMS replica

PDMS oligomer and curing agent (Sylgard 184, silicone elastomer kit, Dow Corning, Midland, MI, USA) was blended in a 10:1 (w/w) ratio. Prior to decanting PDMS against the positive relief, the bubbles arising from mixing was removed via evacuation (RV-12, Edwards, UK) by

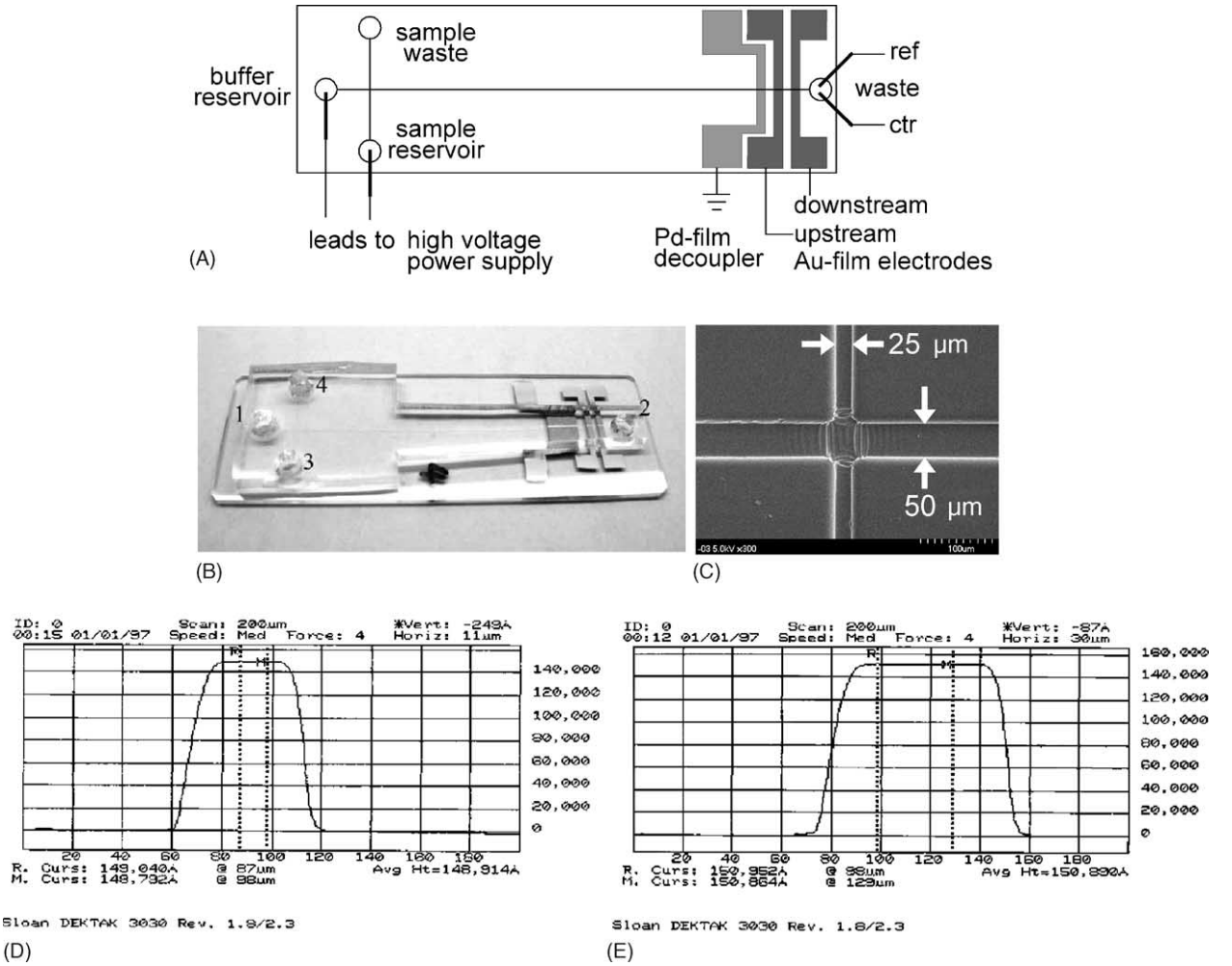

Fig. 1. The electrophoretic chip and channel dimensions. (A) Layout of the electrophoretic chip. (B) A photograph of the microfluidic chip where 1, 2, 3, and 4 represent buffer reservoir, waste, sample reservoir, and sample waste, respectively. (C) An SEM micrograph of the PDMS substrate around the cross-region. In this example, the widths for the injection and separation channels were 25 and 50 μm, respectively. Chips with other dimensions were also used in this study. Section profiles of the positive relief for another design at the (D) injection and (E) separation channels on the patterned glass slide. The height of the positive relief (or the channel depth) was controlled by etching time. In this example, the height was 15 μm. The shapes of the channels were better defined than those shown in our previous publication in which the chips were made of PMMA by pressurization against a tungsten rod (diameter 90 μm) [40].

slowly turning on the vacuum valve until the bubbles were no longer evolving. The mold was cured in an oven at 70 °C for 1 h. The PDMS replica was removed from the master and the wells were created with a hole puncher. The PDMS slab was trimmed with an exacto knife to match the size of the sealing glass slide. The shape of the channels was examined with an optical microscope (HM-2000, HOMA, Taichung, Taiwan). An SEM (S-4700, Type II, Hitachi, Japan) micrograph of the channel is shown in Fig. 1C.

2.1.3. Substrates with metallic films for electrophoresis and electrochemistry

Common 1 in. × 3 in. glass slides were used to seal the PDMS slab and used as the electrode substrates. Prior to being placed in the vacuum chamber of a bell-jar evaporator (nominal pressure of 3×10^{-6} Torr, Auto 306, Edwards High Vacuum International, West Sussex, UK) (1 Torr = 133.32 Pa), the glass slides were cleaned with piranha solution (a 1:3 (v/v) mixture of 30% H_2O_2 and concentrated H_2SO_4, which reacts violently with organic materials and should be handled with great care). A 4–5 nm Cr or Ti underlayer was deposited to enhance the adhesion of the Pd and Au films. The deposition rates for the Pd decoupler and the Au working electrodes were 1–2 and 0.4 nm/s, respectively, monitored by a quartz crystal microbalance (STM-100/MF, Sycon, NY, USA). A piece of Al foil was used as the mask where the pattern was generated with a laser cutting tool. As illustrated in Fig. 1A and B, the sample loading channel and the metallic films were configured perpendicularly to the separation channel.

2.1.4. Bonding procedures for microfluidic chips

The PDMS slab and the glass slides were placed into a plasma generator (Harrick, PDC-32G, Ossining, NY, USA)

where the pressure was pumped down to 80 mTorr and then back-filled with oxygen to 300 mTorr for 1 min. The two pieces were brought to into conformal contact with slight pressure against where the metallic films resided for ca. 30 s. Fig. 1B shows a photograph of a typical microfluidic chip.

2.1.5. Chemicals and solutions

Catecholamines, MES, 3-(cycohexylamino)propanesulfonic acid (CAPS), and other electrolytes were analytical reagent grade and were purchased from Sigma, Aldrich, or Merck. Solutions were prepared with purified water (18 MΩ cm, Millipore-Q, Millipore Inc.). The electrolyte solutions were buffered to desired pH by drop-wise introduction of 5 M NaOH (semiconductor grade, Aldrich). The reported pH and conductivity of the solution was carefully measured with a pH meter (Orion 410, Beverly, MA, USA) and a conductivity meter (Pt electrode; Suntex SC-120 conductivity meter, Taiwan, ROC). Standard solutions of catecholamines with desired concentrations were made fresh daily by serial dilution in the separation electrolyte. Prior to injection, sample and electrolyte solutions were filtered through a 0.45 μm syringe filter (Gelman Sciences Inc.).

2.1.6. Apparatus

The high voltage dc power supply utilized in the sample loading and electrophoretic separation was a Keithley 237, a high voltage source-measure unit that the input voltages and output electrophoretic currents were monitored digitally so as to improve the reproducibility of the experiments. (Warning: to avoid electrical shock, the microchip device should be isolated in a Plexiglas box and the high voltage power supply should be handled with extreme care.) Amperometric measurements were performed with either one or two LC-4C potentiostats (Bioanalytical Systems, West Lafayette, IN, USA). The former operated with a quasi-dual mode in which only one working electrode provided a high-quality filtered output, while in the latter one each LC-4C independently controlled its assigned working electrode. Outputs of redox current were connected to a PC (Pentium II MMX 233 MHz) equipped with a dual-channel data acquisition interface card (model ChemLab 9724-2, Scientific Information Service Corp., Taipei, Taiwan, ROC). Simultaneously monitoring with the faradaic currents, the applied electrophoretic voltage and current were recorded via another interface card (IEEE-488, National Instruments) controlled by a software named *Testpoint* in some of the experiments. The reference electrode was a standard Ag/AgCl (model: RE-5B, Bioanalytical Systems) and the counter electrode was a Pt wire. Both electrodes were placed in the buffer waste reservoir. Cyclic voltammetry was performed with a CHI model 421 potentiostat (CH Instruments, Austin, TX, USA).

2.2. Electrophoresis procedures

2.2.1. Solution filling

For 75 μm width channel, the PDMS channels were filled with electrolytes via a syringe manually as the general procedures for fused silica capillaries. However, due to the hydrophobic nature of PDMS, such a protocol was difficult to inject aqueous solutions into channels with the width equal to or narrower than 50 μm. Either the back pressure was too large to load in the solution or there were bubbles lodged at the rims of the channels. A vacuum-filling method developed by Nuzzo and co-workers was adapted here and the results were satisfactorily [52]. The microfluidic device was placed in a vacuum desiccator and the wells were filled with CE electrolytes (0.05 ml). The pressure was slowly pumped down to 50 Torr for 5 min using a mechanical pump (RV-12, Edwards, UK) equipped with a liquid nitrogen trap. As the pressure in the desiccator was decreased, gas in the channels escaped into the wells and the solutions were back filled.

2.2.2. Electrophoretic procedure

Prior to electrophoresis, the channels were flushed sequentially with 0.01 M NaOH, deionized water, 0.01 M NaOH, deionized water, and then with separation electrolyte twice. The solutions in the reservoirs were changed when the electrophoretic current became stable. Before the repetitive run got started, the channel for sample injection (the channel between wells 3 and 4 in Fig. 1B) was filled electrokinetically with the sample solution by applying a driving voltage between well 3 and the Pd film until the amperometric signal was detected at the working electrode. The excess analytes in the separation channel were drained by applying a high voltage, typically 400 V/cm, between the buffer reservoir (well 1) and the Pd decoupler until the EC current returned to baseline, indicating the passage of the analytes over the working electrodes [26–30,37]. Subsequent sample loading and separation were repetitively performed by applying electric field of 400 V/cm between sample reservoir (well 3) and the Pd decoupler for 2.7 s, and then applying separation voltage between the buffer reservoir (well 1) and the Pd decoupler.

3. Results and discussion

Fig. 1 represents an example of the microfluidic chips, including the chip layout, a photo of the completed device, an SEM picture showing the channel widths, and α-step profilograms of the channel depths. The channels were poly(dimethyl)siloxane (PDMS) molded from a positive relief and bonded onto a 1 in. × 3 in. glass slide pre-patterned with Pd and Au metallic films. The fabrication procedures are described in Section 2. The results demonstrate that the channel dimensions of the microfluidic devices used here are well defined.

3.1. Performance of Pd decoupler

Fig. 2 shows the correlation of electrophoretic current with the strength of electric field measured between the electrolyte reservoir and the Pd film (film thickness: 506 Å) in

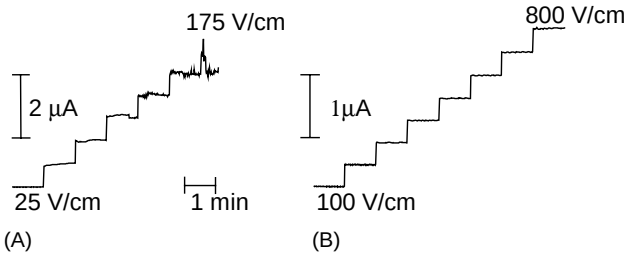

Fig. 2. Influence of the electric field on hydrogen dissipation at the Pd decoupler. Presented are typical traces of electrophoresis current measured in (A) 10 mM NaOH and (B) 20 mM MES. From bottom to top, the strength of electric field increases from 25 to 175 V/cm in 25 V/cm step for (A) and from 100 to 800 V/cm in 100 V/cm step for (B). The channel dimension (trapezoid: long side × short side × depth) and the thickness of the Pd film were 75 μm × 37 μm × 26 μm and 506 Å, respectively.

10 mM NaOH (κ = 2.00 mS/cm) and in 20 mM MES (pH 5.5, κ = 0.262 mS/cm), respectively, representative behaviors at high and low conductivity levels of CE electrolytes. In Fig. 2A, the strength of applied electric field was increased from 25 in 25 V/cm steps and the electrophoretic current increased proportionally. The solution resistivity within the channel was about 35 MΩ. At a higher electric field of 175 V/cm, the current fluctuated vigorously and the Pd film appeared relatively less shiny and slightly opaque, indicating that the rate of hydrogen evolving exceeded that of dissipating. The trace in Fig. 2B was measured with increments of 100 V/cm and maintains an Ohmic response throughout the examined range from 100 to 800 V/cm. The solution resistivity obtained from Fig. 2B is 28 GΩ/cm.

To learn the practicability and applicability of such microfluidic devices in CE separation, exploration of the electrophoretic traces the same as those in Fig. 2 was carried out on several common CE electrolytes. Summarized in Table 1 are the upper limits of the electric field practical for holding stable electrophoretic currents. Strong electrolytes exhibited lower limits, a result of a hydrogen evolving rate faster than that of hydrogen dissipating through the Pd decoupler. The upper limits were raised by thickening the Pd film, suggesting that the rate of hydrogen dissipation was promoted by increasing the Pd volume. Alternatively, with the diminution of the channel dimension and thus the increase of channel resistance, the upper limits were improved. Although a few tries at 1200 V/cm exhibited stable response in low conductive media, electric fields stronger than 800 V/cm were not intentionally examined. Under general CE conditions, Pd and Au films remain intact after repetitive operations for more than 100 runs.

3.2. Performance of the EC detection

In end-column detection (namely, CE–EC without the decoupler), the high electric field distorts the voltammetric waveforms of analytes and thus hydrodynamic voltammograms (HDVs) are generally performed to find the proper potential setting for the working electrode. A series of electropherograms obtained at the upstream electrode is displaced in Fig. 3A where the potentials at the upstream ($E_{upstream}$) and downstream ($E_{downstream}$) electrodes were incrementally changed from −0.1 to 0.6 V and fixed at −0.3 V, respectively. The thickness of the Pd film was 960 Å and the channel dimensions were 75 μm × 37 μm × 26 μm (trapezoid: long side × short side × depth). The redox species, 100 μM dopamine (DA) and catechol (CA), were measured under the electric field of 400 V/cm. Their peak currents reached plateau at +0.4 V, about 0.1–0.4 V less positive than reports of end-column detection. Note that the working electrode was placed in the channel and that the cross-sectional area of the channel was ca. three-fold larger than that of the 25 μm i.d. capillary commonly used for end-column detection. Fig. 3A demonstrates that the effect of the electric field on amperometric detection is insignificant. Likewise, by fixing the potential of the upstream electrode at +0.4 V, the HDVs for the downstream electrode were collected and presented in Fig. 3B. The HDVs obtained under the electric fields of 200 and 600 V/cm were only slightly different than that of 400 V/cm.

For conditions the same as those of Fig. 3 except that the potential settings were +0.5 V for $E_{upstream}$ and −0.4 V for $E_{downstream}$, the linear range, sensitivity, limit of detection (S/N), and number of theoretical plates for DA are 0.5–50 μM, 47 pA/μM, 0.25 μM, and 7000 m^{-1}, respectively.

Table 1
Correlation between channel dimension, thickness of Pd films, CE electrolytes, and upper limits of electric field (V/cm)[a] for electrophoresis

Solution (mM)	pH	Conductivity (mS/cm)	75 × 26[b]				25 × 15[b]			
			506[c]	762[c]	960[c]	1155[c]	506[c]	762[c]	960[c]	1155[c]
NaOH (10)	–	2.00	150	800	800	800	450	800	800	800
CAPS (100)	10.4	1.90	400	800	800	800	700	800	800	800
Borate (15)	8.7	2.52	105	190	200	220	120	220	220	240
MES (100)	5.5	1.10	600	800	800	800	800	800	800	800
Phosphate (20)	5.5	1.50	150	350	380	450	225	460	480	500
Acetate (100)	4.8	4.04	<100	120	120	130	100	160	160	180
Citrate (20)	2.5	1.13	550	800	800	800	775	800	800	800

[a] Upper limit of 800 V/cm denotes that electrophoresis was stable at least at 800 V/cm because higher electric fields were not deliberately inspected.
[b] Dimension of separation channel (width × depth, μm).
[c] Palladium thickness (Å).

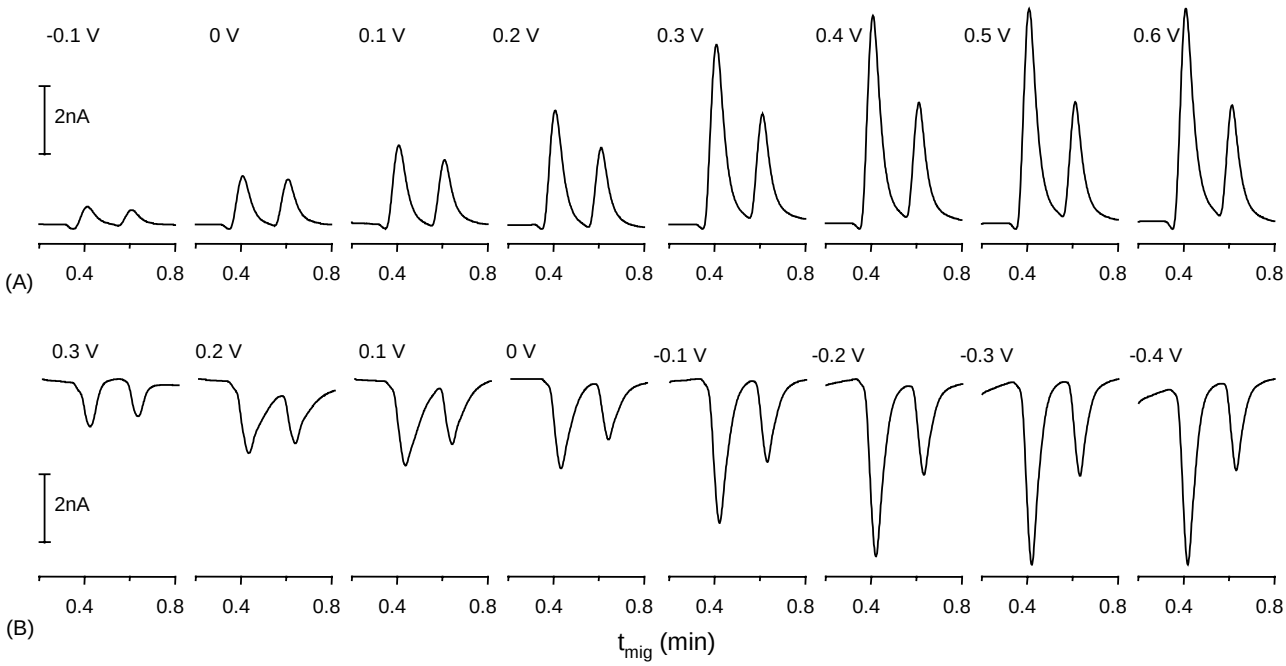

Fig. 3. Electropherograms obtained at (A) the upstream electrode and (B) the downstream electrode for HDVs. The voltages denoted in the figure were the potentials at the (A) upstream and (B) downstream electrodes. The potentials at the downstream and upstream electrode were parked at (A) −0.3 V and (B) +0.4 V, respectively. Conditions: channel length, 5 cm; channel dimension (trapezoid: long side × short side × depth), 75 μm × 37 μm × 26 μm; Pd-film thickness, 96 nm; film spacing: Pd–$Au_{upstream}$: 1 mm, $Au_{upstream}$–$Au_{downstream}$: 1 mm; separation, 400 V/cm; injection, 400 V/cm, 2.7 s; redox species, 100 μM DA, 100 μM CA; electrolyte, 25 mM MES, pH 5.5, 0.31 mS/cm.

The corresponding figures for CA are 1.0–100 μM, 28 pA/μM, 0.49 μM, and 15 000 m^{-1}, respectively. The amperometric background in CE–EC is generally perturbed upon switching on and off the electric field for sample injection and separation. For this Pd decoupler device, the fluctuation of the background was acceptable. For example, the amperometric pulse due to toggling the electric field on and off up to 600 V/cm was well below 1 nA. Also evident in Fig. 3 was that the pulse returned to the baseline level typically within 0.3 min, demonstrating the feasibility of employing the Pd-film decoupler for fast CE–EC detection. The electric pulse, however, could be problematic for detection of sub-μM level analytes. At sub-nanoampere scale, the tilt of the baseline appeared pronounced and thus the lower boundary of detection was limited to ca. 0.25 μM for DA and 0.49 μM for CA.

3.2.1. Amperometric enhancement of the in-channel dual-EC detection

The electropherogram of DA and CA shown in Fig. 4A was obtained with the single-electrode detection scheme where the downstream electrode was not connected to the potentiostat. The coulometric efficiencies, estimated by the charge ratio of integrated peak area to that of injected amount [50], for DA and CA, were about 21 and 23%, respectively. Because the position of the sample front at the channel cross was essentially receding during separation, the efficiency values were underestimated as pointed out by other groups [14,29]. Considering the high electric field and fast linear velocity (12.5 cm/min), the coulometric efficiency was high, a result of a relatively large electrode area and a confined space around the electrode in the microchannel chip [51]. When a reduction potential of −0.3 V was applied to the downstream electrode, the amperometric signal at the upstream electrode was, surprisingly, amplified ca. 2.75 folds for 20 μM DA and CA (Fig. 4B). The reduction current measured at the downstream electrode was also larger than the

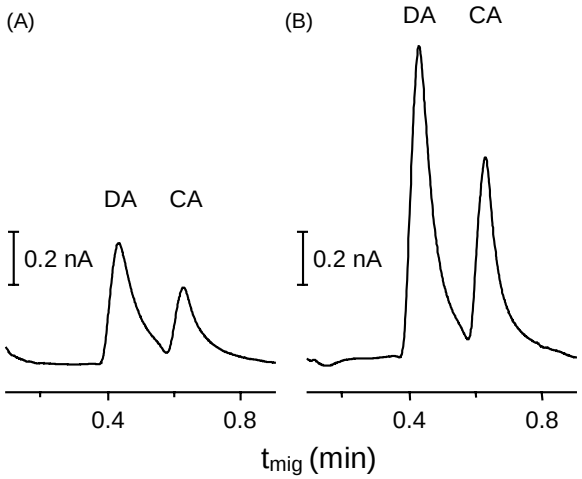

Fig. 4. Electropherograms obtained with detection modes of (A) single electrode and (B) dual-series electrodes. Conditions: solutes, mixture of 20 μM DA and 20 μM CA; potential settings: $E_{upstream}$: +0.4 V, $E_{downstream}$: −0.3 V; other conditions, the same as Fig. 3.

Table 2
Enhancement ratio of i_{dual} to i_{single} at the upstream electrode

Concentration (μM)	i_{single} (nA)		i_{dual} (nA)		i_{dual}/i_{single}	
	DA	CA	DA	CA	DA	CA
5	0.140	0.074	0.272	0.143	1.94	1.93
10	0.230	0.140	0.560	0.309	2.43	2.21
20	0.426	0.254	1.17	0.669	2.75	2.63
40	0.680	0.416	2.25	1.30	3.31	3.13
50	0.741	0.454	2.63	1.50	3.55	3.30
60	0.816	0.505	3.06	1.76	3.75	3.49

Experimental conditions were the same as those in Fig. 4B.

oxidative current obtained with the single-electrode mode. The former (dual-electrode mode) was roughly 1.5 times that of the latter (single-electrode mode). The collection efficiencies, $i_{downstream}/i_{upstream}$, for DA and CA were ca. 60%. Table 2 summarizes the enhancement ratio which becomes larger at higher concentrations.

When the upstream electrode was set at reduction potential (−0.4 V) under the single-electrode mode, there was no current response because DA and CA were in reduced form. Surprisingly, when the downstream electrode was turned on at oxidizing potentials, reduction current was acquired at the upstream electrode (Fig. 5B) and the oxidation current at the downstream was enhanced. For comparison, shown in Fig. 5A were electropherograms obtained under normal potential settings. This unexpected phenomenon demonstrates that the oxidized species returned from the downstream electrode back to the upstream electrode.

In a simplified CE model, such signal enhancement can not be attributed to analytes recycling between the electrodes because such a fluidic system carries the redox molecules toward the direction of the waste reservoir and, therefore, the molecules reduced at the downstream electrode cannot reach the upstream electrode again. This is apparently not true in this study of CE–EC chips integrated with in-channel dual electrodes. The working electrodes are fabricated such that the sub-micrometer films are kinks positioned perpendicularly to the flow pathway. Considering the fact that flat electroosmotic flow profile becomes parabolic after passing the Pd decoupler and that the hydrodynamic flow velocity near the wall is slow, the edge of the downstream electrode is likely to generate turbulence or swirls which drive the redox species back to the upstream electrodes. Note that the decoupler and the upstream electrodes are also the sources of turbulence. Another plausible cause, raised by one of the reviewers, for the signal enhancement is the hydrogen produced at the Pd decoupler. It is possible that hydrogen does not completely dissipate through the Pd decoupler and is dissolved in the flowing stream. The high reducing power of hydrogen should contribute significantly to the redox event of catecholamines at the working electrodes. To diminish the effect of turbulent flow on signal enhancement, we prepared chips with the downstream electrode spaced 2.0 cm from the upstream electrode. The signal at the upstream electrode was the same as the single-electrode mode and was no longer affected by the potential settings at the downstream electrode. Because the electrodes were still confined within the channel, taking together with the results shown in Fig. 5, the possibility of signal enhancement due to instrumental artifacts is unlikely.

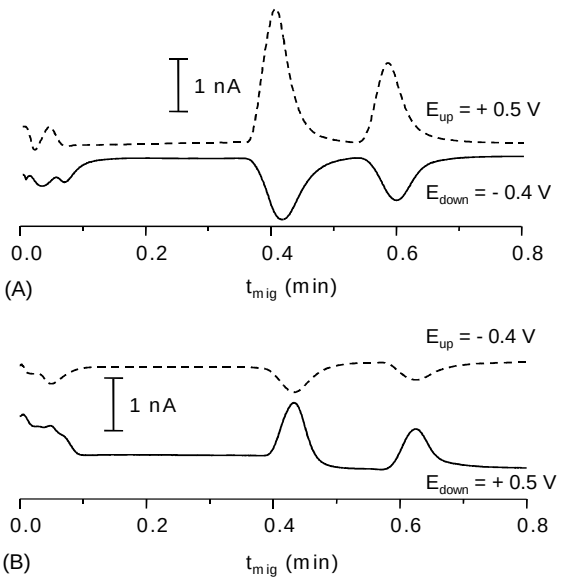

Fig. 5. Electropherograms obtained with (A) normal and (B) reversal potential settings. Conditions: solutes, mixture of 50 μM DA and 50 μM CA; $E_{upstream}$ and $E_{downstream}$: denoted in the figure; other conditions, the same as Fig. 3.

4. Conclusion

We have demonstrated that the Pd decoupler allows the CE–EC chip operated under general strength of electric fields (200–800 V/cm). The coulometric and collection efficiencies for the catecholamines are above 20 and 60%, respectively. The values are larger than those of end-column CE–EC chips due to characteristics of the confined channel. A surprising finding is that the series dual-electrode detection exhibits signal enhancement with respect to that of the single-electrode mode. For the dual-electrode mode, the linear range, sensitivity, limit of detection, and number of theoretical plates for DA and CA are, respectively, 0.5–50 μM, 47 pA/μM, 0.25 μM, 7000 m^{-1}, and 1.0–100 μM, 28 pA/μM, 0.49 μM, 15 000 m^{-1}. We hypothesize that the encounter of the sample zone and the edge of the downstream electrode generates a turbulent flow which carries redox product at the downstream back to the upstream electrode.

Acknowledgements

The authors thank National Science Council and National Nano Device Laboratories for the financial support and facility fabrication of microfluidic chips. Special thanks to Profs.

T.-S. Hsi (National Sun Yat-sen University) and C.-S. Yang (National Chi Nan University) for the fruitful discussions.

References

[1] D.A. Roston, R.E. Shoup, P.T. Kissinger, Anal. Chem. 54 (1982) 1417A.
[2] A.J. Bard, L.R. Faulkner, Electrochemical Methods: Fundamentals and Applications, Wiley, New York, 2001.
[3] S.M. Lunte, C.E. Lunte, P.T. Kissinger, in: P.T. Kissinger, W.R. Heineman (Eds.), Laboratory Techniques in Electroanalytical Chemistry, Marcel Dekker, New York, 1996, p. 813.
[4] B.L. Lin, L.A. Colon, R.N. Zare, J. Chromatogr. A 680 (1994) 263.
[5] M. Zhong, J. Zhou, S.M. Lunte, D.M. Giolando, J.R. Kirchhoff, Anal. Chem. 68 (1996) 203.
[6] F.-M. Matysik, U. Backofen, Fresenius J. Anal. Chem. 356 (1996) 169.
[7] F.-M. Matysik, F. Bjorefors, L. Nyholm, Anal. Chim. Acta 385 (1999) 409.
[8] P.D. Voegel, R.P. Baldwin, Electrophoresis 19 (1998) 2226.
[9] M. Zhong, S.M. Lunte, Anal. Chem. 71 (1999) 251.
[10] L.A. Holland, S.M. Lunte, Anal. Chem. 71 (1999) 407.
[11] D.-c. Chen, S.-S. Chang, C.-h. Chen, Anal. Chem. 71 (1999) 3200.
[12] Z. Liu, O. Niwa, R. Kurita, T. Horiuchi, Anal. Chem. 72 (2000) 1315.
[13] Z. Liu, O. Niwa, R. Kurita, T. Horiuchi, J. Chromatogr. A 891 (2000) 149.
[14] R.S. Martin, A.J. Gawron, S.M. Lunte, C.S. Henry, Anal. Chem. 72 (2000) 3196.
[15] A.J. Gawron, R.S. Martin, S.M. Lunte, Electrophoresis 22 (2001) 242.
[16] R.S. Martin, A.J. Gawron, B.A. Fogarty, F.B. Regan, E. Dempsey, S.M. Lunte, Analyst 126 (2001) 277.
[17] Q. Weng, W. Jin, J. Chromatogr. A 971 (2002) 217.
[18] D.J. Harrison, K. Fluri, K. Seiler, Z. Fan, C.S. Effenhauser, A. Manz, Science 261 (1993) 895.
[19] D.J. Harrison, A. Manz, Z. Fan, H. Ludi, H.M. Widmer, Anal. Chem. 64 (1992) 1926.
[20] S.A. Soper, S.M. Ford, S. Qi, R.L. McCarley, K. Kelly, M.C. Murphy, Anal. Chem. 72 (2000) 643A.
[21] W.R. Vandaveer IV, S.A. Pasas, R.S. Martin, S.M. Lunte, Electrophoresis 23 (2002) 3667.
[22] A.T. Woolley, K.Q. Lao, A.N. Glazer, R.A. Mathies, Anal. Chem. 70 (1998) 684.
[23] J.S. Rossier, M.A. Roberts, R. Ferrigno, H.H. Girault, Anal. Chem. 71 (1999) 4294.
[24] A. Hilmi, J.H.T. Luong, Anal. Chem. 72 (2000) 4677.
[25] J.S. Rossier, R. Ferrigno, H.H. Girault, J. Electroanal. Chem. 492 (2000) 15.
[26] N.A. Lacher, K.E. Garrison, R.S. Martin, S.M. Lunte, Electrophoresis 22 (2001) 2526.
[27] U. Backofen, F.-M. Matysik, C.E. Lunte, Anal. Chem. 74 (2002) 4054.
[28] J. Wang, B.M. Tian, E. Sahlin, Anal. Chem. 71 (1999) 5436.
[29] J. Wang, B.M. Tian, E. Sahlin, Anal. Chem. 71 (1999) 3901.
[30] S.-C. Wang, C.E. Perso, M.D. Morris, Anal. Chem. 72 (2000) 1704.
[31] M. Pumera, J. Wang, E. Grushka, R. Polsky, Anal. Chem. 73 (2001) 5625.
[32] J. Wang, M. Pumera, Anal. Chem. 74 (2002) 5919.
[33] J. Wang, G. Chen, M.P. Chatrathi, A. Fujishima, D.A. Tryk, D. Shin, Anal. Chem. 75 (2003) 935.
[34] R.S. Martin, K.L. Ratzlaff, B.H. Huynh, S.M. Lunte, Anal. Chem. 74 (2002) 1136.
[35] P.F. Gavin, A.G. Ewing, J. Am. Chem. Soc. 118 (1996) 8932.
[36] P.F. Gavin, A.G. Ewing, Anal. Chem. 69 (1997) 3838.
[37] J.A. Lapos, D.P. Manica, A.G. Ewing, Anal. Chem. 74 (2002) 3348.
[38] C.-C. Wu, R.-G. Wu, J.-G. Huang, Y.-C. Lin, H.-C. Chang, Anal. Chem. 75 (2003) 947.
[39] D.M. Osbourn, C.E. Lunte, Anal. Chem. 75 (2003) 2710.
[40] D.-c. Chen, F.-L. Hsu, D.-Z. Zhan, C.-h. Chen, Anal. Chem. 73 (2001) 758.
[41] W.T. Kok, Y. Sahin, Anal. Chem. 65 (1993) 2497.
[42] X. Huang, W.T. Kok, J. Chromatogr. A 716 (1995) 347.
[43] H. Natter, B. Wettmann, B. Heisel, R. Hempelmann, J. Alloys Compound 253–254 (1997) 84.
[44] G.L. Powell, J.R. Kirkpatrick, Phys. Rev. B 43 (1991) 6968.
[45] A. Kufudakis, J. Cermak, F.A. Lewis, Z. Phys. Chem. 164 (1989) 1013.
[46] L. Martynova, L.E. Locascio, M. Gaitan, G.W. Kramer, R.G. Christensen, W.A. Maccrehan, Anal. Chem. 69 (1997) 4783.
[47] L.E. Locascio, C.E. Perso, C.S. Lee, J. Chromatogr. A 857 (1999) 275.
[48] Y.-H. Chen, W.-C. Wang, K.-C. Young, T.-T. Chang, S.-H. Chen, Clin. Chem. 45 (1999) 1938.
[49] D.C. Duffy, J.C. McDonald, O.J.A. Schueller, G.M. Whitesides, Anal. Chem. 70 (1998) 4974.
[50] S. Sloss, A.G. Ewing, Anal. Chem. 65 (1993) 577.
[51] K. Ueno, H.-B. Kim, N. Kitamura, Anal. Chem. 75 (2003) 2086.
[52] J. Monahan, A.A. Gewirth, R.G. Nuzzo, Anal. Chem. 73 (2001) 3193.